Spatial and temporal distribution of fine aerosol acidity in the Eastern Mediterranean

Anna Maria Neroladaki[1,2], Maria Tsagkaraki[1], Kyriaki Papoutsidaki[1], Kalliopi Tavernaraki[1], Filothei Boufidou[3], Pavlos Zarmpas[1], Irini Tsiodra[4], Eleni Liakakou[4], Aikaterini Bougiatioti[4], Giorgos Kouvarakis[1], Nikos Kalivitis[1], Christos Kaltsonoudis[2], Athanasios Karagioras[5], Dimitris Balis[6], Konstantinos Michailidis[6], Konstantinos Kourtidis[5], Stelios Myriokefalitakis[4], Nikos Hatzianastassiou[7], Spyros N. Pandis[2], Athanasios Nenes[2,8], Nikolaos Mihalopoulos[1,3] and Maria Kanakidou[1,2,7]

[1]Environmental Chemical Processes Laboratory (ECPL), Department of Chemistry, University of Crete, 70013 Heraklion, Greece

[2]Center for Studies of Air Quality and Climate Change, Institute for Chemical Engineering Sciences, Foundation for Research and Technology Hellas, 26504 Patras, Greece

[3]Institute of Environmental Physics, University of Bremen, 28359 Bremen, Germany

[4]Institute for Environmental Research and Sustainable Development, National Observatory of Athens, 15236 Palea Penteli, Greece

[5] Department of Environmental Engineering, Democritus University of Thrace, 67100 Xanthi, Greece

[6]Laboratory of Atmospheric Physics, Aristotle University of Thessaloniki, 54634 Thessaloniki, Greece

[7]Laboratory of Meteorology, Department of Physics, University of Ioannina, 45110 Ioannina, Greece

[8]Laboratory of Atmospheric Processes and their Impacts, School of Architecture, Civil and Environmental Engineering, Ecole Polytechnique Fédérale de Lausanne, 1015, Lausanne, Switzerland

Correspondence to: Maria Kanakidou (mariak@uoc.gr)

Abstract. Aerosol acidity (pH) affects aerosol composition and properties, and therefore climate, human health and ecosystems. Fine aerosol acidity and its seasonal variation at 6 sites (Finokalia, Patras, Thissio, Ioannina, Thessaloniki, and Xanthi) in Greece were investigated during 2019-2020. The thermodynamic model ISORROPIA-lite was used to calculate aerosol water and acidity based on measurements of the chemical composition of $PM_{2.5}$ and available gas-phase concentrations of HNO_3, NH_3, and HCl. During winter the fine aerosols were acidic to moderately acidic throughout Greece with an overall mean aerosol pH of 3.57±0.44 in urban areas and 3.05±0.50 in remote locations. The highest aerosol pH (4.08±0.42) in January 2020 was found in Ioannina due to, among others, high K^+ levels from biomass burning emissions. Aerosols in Xanthi were the most acidic due to high sulfate levels. Similar seasonal profiles of aerosol pH were observed at all sites studied with different factors contributing to this seasonality. During the summer $PM_{2.5}$ at Thissio, Ioannina and Finokalia was acidic with a mean aerosol pH across all three sites of 1.76±0.40. During this season, sulfates were the driver of the higher acidity conditions at Thissio and Finokalia, with other factors such as the semivolatiles and temperature contributing to a lesser extent. At Ioannina, temperature along with the total ammonia and nitrate were the main contributors to the seasonal difference of the aerosol pH, while some of the nonvolatile species also contributed. In most cases, the importance of organics for aerosol pH was small.

1 Introduction

42   The aerosol pH is one of the most important chemical properties of aerosols. It controls the rates of several

43   reactions in the particulate phase (e.g., sulfate and oligomer formation reactions in the particulate phase) and

44   governs the gas-particle partitioning of semivolatile gases such as ammonia (NH_3), nitric acid (HNO_3) and

45   hydrochloric acid (HCl), and some organic acids with low molecular weight (formic, oxalic, acetic etc.) and bases

46   (e.g. amines). Several studies have thoroughly discussed the importance of the gas phase NH_3 and HNO_3 and their

47   effect on the particulate matter as well as their relationship with aerosol pH and water (Pye et al., 2020; Nenes et

48   al., 2020; Guo et al., 2018, 2016, 2017b). NH_3 from anthropogenic and biogenic emissions is the most important

49   gaseous base in the atmosphere, while HNO_3 is an acid produced by the oxidation of NO_x mainly emitted by

50   combustion sources (Seinfeld and Pandis, 2006). HNO_3, because of its strong acidity and solubility, partitions

51   more in the gas phase than in the particle phase (as nitrate) at lower aerosol pH (usually below 1.5 to 2) (Weber

52   et al., 2016), while NH_3 remains in the gas phase at higher pH. These processes have serious implications for the

53   wet and dry deposition of these semivolatile pollutants on ecosystems, their lifetime, climate and human health

54   (Pye et al., 2020).

55   Metal cations, including those that originate from dust and sea salt, are nonvolatile at atmospheric

56   temperatures. These constituents seriously affect the aerosol pH together with parameters such as the

57   meteorological conditions (i.e. temperature and relative humidity). These parameters and the availability of

58   sulfuric acid (that partitions almost exclusively to the particulate phase) are mostly responsible for the wide range

59   of the pH of atmospheric particles (Pye et al., 2020).

60   Aerosol pH affects the uptake of sulfur dioxide (SO_2) into the aerosol aqueous phase and its oxidation to sulfate

61   (Seinfeld and Pandis, 2006). This is important for climate, as sulfate is one of the main scattering components of

62   atmospheric aerosols with a cooling effect on climate. Acid catalyzed reactions lead to the formation of brown

63   carbon that is an important contributor to absorbing aerosol (Zhang et al., 2020). Atmospheric acidity affects

64   aerosol toxicity, controlling the solubilization of toxic forms of transition and heavy metals, such as copper and

65   iron (Fang et al., 2017) with adverse impacts on human health (Vierke et al., 2013). Furthermore, acidity increases

66   the solubility and thus the bioavailability of iron, phosphorus and trace metals that are deposited on ecosystems

67   (Pye et al., 2020). This is of a great importance in oligotrophic areas, such as the East Mediterranean Sea, a marine

68   desert, characterized by extremely low biological productivity, due to the limited availability of nutrients like

69   phosphate (Powley et al., 2017). The area is frequently influenced by dust outbreaks from the Saharan desert,

70   which contain several minerals and metals primarily in insoluble forms. The conversion of insoluble to soluble

71   bioavailable form of a given nutrient is favored under acidic conditions (Kanakidou et al., 2018; Nenes et al.,

72   2011). The solubility of iron and thus its bioavailability to ecosystems, is also controlled by acidity, as it is

73   enhanced in the presence of acidic species. Theodosi et al. (2008) found that in the Eastern Mediterranean the iron

74   solubility ranged from 28% for polluted rainwater (pH 4-5) to 0.5% for Sahara dust episodes (pH=8).

75   Although the acidity of atmospheric particles plays such a critical role in all of the atmospheric processes

76   mentioned above, there is no direct method for its accurate measurement due to the miniscule sample mass and

77   liquid volume (Pye et al., 2020). Thus, several indirect methods have been developed, which estimate aerosol

78   acidity (Pye et al., 2020). One of the best available methods is the aerosol pH prediction using atmospheric aerosol

79   thermodynamic models in combination with measurements of aerosol composition and gas-phase HNO_3, NH_3 and

80   HCl concentrations. Models such as ISORROPIA II (Fountoukis and Nenes, 2007), MOSAIC (Zaveri et al.,

81   2008), E-AIM; (Clegg et al., 2001; Wexler and Clegg, 2002), etc. can be used to this purpose.

Aerosols' acidity covers a wide range and aerosol pH can be as high as about 7 pH units (sea salt), and as low as -1 and sometimes even -2 pH units, depending on the composition of the aerosol and the meteorological conditions in a given area (Pye et al., 2020). Negative values appear when sulfates are the dominant constituent of particulate matter, while the aerosol pH rarely rises above neutral levels (pH = 7). Globally fine atmospheric particles ($PM_{2.5}$) have been found to have a bimodal acidity pattern with one population of smaller particles having an average pH between 1 and 3 pH units, and another of larger particles with a mean pH close to 4 and 5 units, which is due to the influence of dust, sea spray and biomass burning (Sindosi et al., 2012; Pye et al., 2020).

Several studies have investigated the levels of the acidity of fine particles and their major drivers at specific sites. For instance, studies in Beijing and close-by locations indicate a mean wintertime $PM_{2.5}$ pH of 4.2 to 4.9 units (Liu et al., 2017; Guo et al., 2017a; Shi et al., 2017; Ding et al., 2019). Pye et al. (2020) summarized and investigated the fine aerosol pH in several regions globally and reported that overall aerosol pH is consistently acidic and looking into the seasonality, during wintertime where low temperature and high relative humidity occur, aerosol pH was higher compared to summertime following the temperature and the availability of liquid water content. Tao and Murphy (2019) reported that in winter the pH of fine aerosols was around 3 units at 6 sites in Canada and was strongly influenced by temperature, relative humidity and aerosol chemical composition. Kakavas et al. (2021) simulated the aerosol acidity and its variation with size and altitude over Europe during summer and found the ground level mean aerosol pH across the domain to be 2.05 for PM_1, 2.65 for $PM_{1-2.5}$, 3.2 for $PM_{2.5-5}$ and 3.35 for PM_{5-10}. The lowest aerosol pH was reported in the Mediterranean and especially in the eastern Mediterranean where high sulfate and nitrate levels were predicted. This study suggests that Eastern Mediterranean can be an especially interesting region for aerosol pH studies.

There have been only limited estimations of aerosol acidity in the eastern Mediterranean. The $PM_{2.5}$ pH in 6 cities in the eastern Po Valley in Italy (Masiol et al., 2020) was found to range from 1.5 to 4.5 with summer minima and winter maxima and mean pH values across all sites of 2.2 ± 0.3 and 3.9 ± 0.3, respectively. These levels of fine aerosol acidity were mainly driven by secondary sulfate, fossil fuel combustion, secondary nitrate and biomass burning. An earlier study in the same area (Squizzato et al., 2013) investigated seasonally the aerosol pH and found that in spring the aerosol pH was higher compared to summer (average aerosol pH across the sites; spring 3.6 pH units, summer 2.3, autumn 3, winter 3.6) as a result of desert dust aerosol originating from the Sahara desert. Again in Po Valley, a multiyear (25 years) trend of fog water pH and aerosol pH was estimated (Paglione et al., 2021) and an opposite trend between them was found; there was an increase in the fog water pH and a decrease in fine aerosol acidity. In fact, there was a decrease of 0.5-1.5 pH units in the aerosol pH that was driven by the contemporary decrease of the corresponding air pollutants due to environmental policies in combination with the changing meteorology (temperature and relative humidity levels). Lastly, the submicron aerosol pH was estimated in a study conducted at the Finokalia atmospheric observation station in Greece (Bougiatioti et al., 2016) and was found to be highly acidic ranging from 0.5 to 2.8 pH units with daytime minimum and nighttime maximum values due to low aerosol water content and high temperatures during the day. They also pointed out the influence of biomass burning which increased the aerosol pH values highlighting the impact of nonvolatile cations, mainly potassium from biomass burning together with ammonia and nitrate emitted from wood burning. Despite these studies, the spatial distribution of aerosol acidity based on atmospheric composition observations is not well understood.

121   The present study aims to provide a spatial and seasonal picture of the acidity of fine ($PM_{2.5}$) atmospheric

122   aerosol over Greece in the eastern Mediterranean based on observations of atmospheric composition. For this, the

123   ISORROPIA-lite thermodynamic equilibrium model (Kakavas et al., 2022) is used together with observations of

124   the chemical composition of the fine aerosol from 6 sites over Greece and with gas phase NH_3 and HNO_3 data,

125   where available. The water and pH of the fine aerosol are estimated during summer 2019 and winter 2019-2020.

126   The factors controlling the seasonality of aerosol pH are examined and the effect of particulate organic matter on

127   aerosol pH predictions is also investigated.

128   **2 Measurements and Methodology**

129   2.1 Measurement sites

130   Measurements of the chemical composition of $PM_{2.5}$ were performed at 6 sites across Greece (Fig. 1) (Finokalia,

131   Thissio, Patra, Ioannina, Xanthi and Thessaloniki, Table S1). The corresponding summer and winter field

132   campaigns were conducted within the PANACEA (PANhellenic infrastructure for Atmospheric Composition and

133   climatE chAnge) project during the summer of 2019 (at 3 of the sites, Finokalia, Thissio and Ioannina) and the

134   winter of 2019-2020 (at all sites).

135   The Finokalia atmospheric observatory of the University of Crete in Crete, Greece (FKL, 35.33° N, 25.67° E;

136   250 m a.s.l) is a remote regional background site in the northeast coast of the island of Crete (south Greece). The

137   site is not subject to any major anthropogenic influence and it is considered as a representative background site

138   for the entire eastern Mediterranean. During the warm months of the year (April to September, dry season) the

139   station mainly receives air masses from the N/NW (originating from the Central and Eastern Europe and the

140   Balkans), while between October and April (wet season) air masses coming from the South lead to Saharan dust

141   events (Mihalopoulos et al., 1997).

142   The Thissio Air Monitoring station (THI, 37.97° N, 23.72° E, 105 m a.s.l.) of the National Observatory of

143   Athens, Greece is located approximately 50 m above the mean city level near the historical city center. The station

144   is an urban background site due to its distance from traffic and industrial emission sources and receives air

145   pollutants from various urban and regional sources.

146   The Patras site is located at the Institute of Chemical Engineering Sciences (ICE-HT) of FORTH (Foundation

147   for Research and Technology, Hellas), which is in Platani (PTR, 38.30° N, 21.81° E, 100 m a.s.l.) 8 km from the

148   city center. It is an urban background site. Local sources include transportation, biomass burning (both residential

149   and agricultural) and shipping emissions, while long-range transport is the dominant $PM_{2.5}$ source during most

150   periods (Pikridas et al., 2013).

151   The Xanthi station is operated by the Laboratory of Atmospheric Pollution and Pollution Control Engineering

152   of Atmospheric Pollutants of the Department of Environmental Engineering. The station is located in the

153   Kimmeria DUTH campus (XAN, 41.15° N, 24.92° E; 75 m a.s.l.) almost 2 km from the city of Xanthi in

154   northeastern Greece. The station is a rural site and the edge of a slope facing to the south, 20 km away from the

155   seashore. The Rodopi Mountain Range is located to the north of the station. The prevailing winds that reach the

156   site in winter are fairly stable SW/S/SE during the day, but they change to N/NW at night; the location of the site

157 between mountains and a valley creates a closed circulation cell of valley/land breezes (Kastelis and Kourtidis,
158 2016).

159   The Thessaloniki station at the north of Greece is at the Laboratory of Atmospheric Physics (LAP) which is
160 located at the School of Sciences of the Aristotle University of Thessaloniki (LAP, 40.63°N, 22.95°E; 50m a.s.l.).
161 Thessaloniki is a coastal city at Thermaikos Gulf and is the second largest city in Greece. The site experiences air
162 pollution episodes due to the meteorological conditions over northern Greece; with high pressure, anticyclonic
163 systems and sunny weather in summer, while colder temperatures near the surface and snow occur in winter
164 (Flocas et al., 2009). It is considered as a representative urban station.

165   Ioannina (IOA, 39.653195°N, 20.854208°E) is located in Epirus Region in northwestern Greece, which is
166 separated from the eastern part of the country mainland by the Pindus mountain range (orientated from NW to SE
167 and exceeding 2000 m in height). The sampling station was located at a kindergarten yard, 1.5 km from Ioannina's
168 city center. Ioannina is located on a plateau of about 500 m altitude and is surrounded by mountains. The city is
169 next to the Pamvotis lake and is characterized by frequent fog events in winter, due to increased relative humidity,
170 weak winds and basin-like attributes and winter biomass burning events (Kaskaoutis et al., 2020).

171 2.2 Measurements

172 The PANACEA campaigns took place at the 6 sites discussed above during the summer of 2019 (at FKL, THI,
173 IOA) and the winter of 2019-2020 (at all 6 sites). Atmospheric particles were collected daily on quartz-fiber filters
174 using high-volume or low-volume aerosol samplers depending on the site. A Sunset Organic Carbon (OC)
175 /Elemental Carbon (EC) analyzer was used to determine the concentrations of OC and EC, while the inorganic
176 cations: ammonium (NH_4^+), potassium (K^+), calcium (Ca^{2+}), magnesium (Mg^{2+}), sodium (Na^+) and anions: sulfate
177 (SO_4^{2-}), chloride (Cl^-), nitrate (NO_3^-) were determined using ion chromatography. Details on the methods of the
178 $PM_{2.5}$ filter analysis during the PANACEA winter and summer campaign can be found in (Kaskaoutis et al., 2022).
179 In situ-measurements of temperature and relative humidity were also available for the period of the campaigns
180 (Fig S1 and S2).

181   For the campaign period there were not available gas phase concentrations (NH_3, HNO_3) measurements at any
182 of the 6 sampling sites except PTR (NH_3). Thus, for NH_3, satellite data were used for the remaining sites (except
183 IOA during the winter campaign period). For HNO_3, past in situ measurements were used at FKL and for the other
184 sites (THI, PTR, IOA, LAP, XAN) past in situ measurements conducted at THI were used. A summary of the
185 type of NH_3 and HNO_3 measurement data used (satellite or in-situ, simultaneous or past, same or neighbor site),
186 is presented in Table S2 of the supplement.

187   In more detail, the Patras site as mentioned above, was the only site with available gas-phase NH_3
188 measurements for the studied periods during the 2019-2020 winter campaign, with mean NH_3 concentration of
189 2.54 ± 0.90 μg/m³. At IOA during the wintertime period of the study, neither in situ observations nor satellite data
190 were available and thus NH_3 observations at PTR were used for IOA. Therefore, the mean NH_3 concentration
191 value from PTR dataset was also used for the IOA wintertime simulations.

192   For the other sites (FKL and THI during winter and summer, and LAP and XAN during winter) NH_3 data
193 (level 2 data, version 1.6.3) were used from the Cross-track Infrared Sounder (CrIS) instrument which is deployed
194 on board the Suomi National Polar-orbiting Partnership (SNPP) platform (into an orbit with an altitude of 824 km

195 above the Earth surface) (Shephard and Cady-Pereira, 2015). NH$_3$ values over these sites were obtained from the
196 CrIS Fast Physical Retrieval (CFPR) product, which provides NH$_3$ concentration data for a total of 15 vertical
197 levels, with the value closest to the ground being taken as the near-surface concentration. From the available CrIS
198 near-surface NH$_3$ concentrations within a 50-km diameter area around each site, the value within the pixel at the
199 closest distance to the site is retained (Shephard et al., 2020; Shephard and Cady-Pereira, 2015). The wintertime
200 near-surface NH$_3$ concentrations as derived from CrIS for FKL, THI, XAN and LAP are shown in Fig. 2. For
201 summer at FKL and THI, mean values of summertime near-surface NH$_3$ (from 13/08/2019 to 19/08/2019 for FKL
202 and from 13/08/2019 to 31/08/2019 for THI) are 1.24 ± 0.61 µg/m^3 and 1.32 ± 1.53 µg/m^3 respectively, were used
203 due to the scarcity of summertime data from CrIS in 2019.

204 For IOA during summer, a mean NH$_3$ concentration of 1.04 µg/m^3 was used as derived from the Atmospheric
205 Infrared Sounder (AIRS) aboard NASA's Aqua satellite (Level 3 data) operating from September 2002 to August
206 2016 (Warner et al., 2016) (the mean summertime 2002-2016 concentration was used).

207 For HNO$_3$ and HCl gas-phase concentration measurements, samples were collected only at Finokalia (2015 -
208 2016) using glass fiber filters coated with Na$_2$CO$_3$ and were analyzed by ion chromatography. The median of
209 these gas-phase measurements of HNO$_3$ and HCl were used here (0.63 µg/m^3 and 0.98 µg/m^3 for winter and 0.95
210 µg/m^3 and 1.34 µg/m^3 for summer, respectively). For all other sites, gas-phase measurements of HNO$_3$ conducted
211 at Thissio from 12/2014 to 3/2016 (Liakakou et al., 2022) were used here as mean values (0.53 ± 0.12 µg/m^3 for
212 winter and 0.91 ± 0.29 µg/m^3 for summer).

213 Since the NH$_3$ in situ observations at PTR did not coincide with any CrIS or AIRS data, a comparison between
214 in situ and satellite data was not possible. The sensitivity of our pH estimates to these assumed NH$_3$ and HNO$_3$
215 concentrations will be examined in a subsequent section (see section 3.4).

216

217 2.3 pH Estimation

218 The pH of the fine aerosol at the 6 studied sites, was calculated using ISORROPIA-lite thermodynamic model
219 (Kakavas et al., 2022), which is an extension of the ISORROPIA-II model (Fountoukis and Nenes, 2007).
220 ISORROPIA-lite treats the same system of aerosols as ISORROPIA-II (Ca^{2+}, K$^+$, Mg^{2+}, SO$_4^{2-}$, Na$^+$, NH$_4^+$, NO$_3^-$,
221 Cl$^-$, H$_2$O and their equilibrium with the gas phase HNO$_3$, NH$_3$, HCl and H$_2$O) with the addition of the organic
222 aerosol and considering only the deliquescent aerosol at all RH values. The addition of organic matter in the
223 thermodynamic equilibrium aerosol system, results in more aerosol water which favors the partitioning of
224 semivolatile inorganic species into the aerosol phase in order to satisfy the equilibrium (Kakavas et al., 2022).
225 The particle water (W$_{org}$) associated with the organic aerosol is implemented in the model using the hygroscopicity
226 parameter (κ_{org}). The total aerosol water content, i.e. the water associated with the inorganic and organic parts of
227 the aerosol, is the sum of the inorganic and organic water and it is used in the thermodynamic calculations. The
228 aerosol pH is then calculated by:

230
$$pH = -\log_{10} \frac{1000 \, \gamma_{H^+} \, [\mathrm{H}^+_{air}]}{[W_{inorg}] + [W_{org}]}$$

229 (1)

where γ_{H^+} is the activity coefficient of the hydronium ion (H^+) here assumed unity, H^+_{air} is the equilibrium particle hydronium ion concentration per volume air ($\mu g/m^3$), W_{inorg} and W_{org} is the water associated with the inorganic and organic part of the aerosol, respectively (both in $\mu g/m^3$). Thus, the aerosol pH was calculated including the contribution of the organic aerosol hence the aerosol water associated with both inorganic and organic species. Daily values were used as input to the model. These were gas phase (NH_3, HNO_3) and particulate phase (ions and OA) concentrations, OA hygroscopicity and density, and meteorological data (temperature and relative humidity).

To calculate the aerosol water content associated with the organic species, the total organic aerosol concentration (OA) derived from the OC measurements at each site is used together with an OA/OC ratio of 1.8 for all sites. This average ratio is consistent with the results of measurements conducted at the same sites (Florou et al., 2017; Hildebrandt et al., 2011; Kaskaoutis et al., 2020, 2022; Kostenidou et al., 2015; Pikridas et al., 2013; Stavroulas et al., 2019; Tsiflikiotou et al., 2019). The hygroscopicity parameter was set to $\kappa_{org}= 0.16$ for Finokalia as suggested in studies for this site (Bougiatioti et al., 2009; Kalkavouras et al., 2019), and $\kappa_{org}=0.12$ for the other sites (Psichoudaki et al., 2018).

3 Results and Discussion

3.1 Aerosol Composition

The chemical composition and mass concentration of the major species in $PM_{2.5}$ measured during the PANACEA campaigns are summarized in Table 1. The dominant $PM_{2.5}$ component was OA at all sites except FKL, where sulfate dominated both in winter and summer. This is typical for remote background sites (Lemou et al., 2020; Sciare et al., 2008). Higher sulfate levels were present in FKL during summer due to high temperatures and photochemistry, followed by organics (typically consisting 20-30% of the $PM_{2.5}$ mass, Pikridas et al., 2010; Putaud et al., 2004). The highest levels of OA were observed at Ioannina (IOA) during winter. OA represented more than 60% of the $PM_{2.5}$ and was mainly due to residential wood burning emissions while the meteorology and topography of the area facilitated the accumulation of all pollutants (Kaskaoutis et al., 2022). Much lower levels of OA and $PM_{2.5}$ mainly of regional origin, were measured at IOA in the summer (Kaskaoutis et al., 2022). At the three sites where measurements were available in the summer (IOA, FKL, THI), sulfate was a major component of the $PM_{2.5}$ despite their different characteristics. Inorganic $PM_{2.5}$ across all sites in winter was dominated by sulfate except IOA where, interestingly, NO_3^- was the dominant inorganic $PM_{2.5}$ component due to possible high NO_x emissions, or NO_x accumulation in the boundary layer due to low inversion heights and decreased horizontal circulation, the latter due to surrounding mountains. The K^+ levels in IOA were also elevated indicating the influence of biomass burning in the area (Kaskaoutis et al., 2022).

3.2 Aerosol pH across Greece

3.2.1 Winter

The distributions of estimated pH of $PM_{2.5}$ as derived from the ISORROPIA-lite model for the 6 studied sites during winter (January 2020) is shown in Fig. 3a. Due to the lack of data in some of the sites during the winter

266 2019-2020, the results of only January 2020 were used in order to be able to compare the aerosol pH results among
267 the sites. The entirety of the aerosol pH results for all sites during winter 2019-2020 can be found in Fig. S4.

268   In January the aerosols at THI were slightly acidic with a wide range of pH values (2.17 to 4.17), reflecting
269 the variation of the $PM_{2.5}$ composition and meteorology. The mean pH was 3.30 ± 0.48 (median 3.34). Days with
270 highly acidic aerosol, i.e. pH below 2.5, were associated with elevated sulfate levels and northerly winds. At FKL
271 the mean aerosol pH was 3.25 ± 0.37 and ranged from 2.73 to 3.89 (median 3.30). The elevated pH coincided
272 with high concentrations of nonvolatile cations (NVC) and NH_3 and the lower pH values (less than 2.8) occurred
273 during periods with high levels of sulfates. In the northern part of Greece, at XAN the pH range covered 2.24
274 units with a mean value of 2.81 ± 0.53 (median 2.69). The shift between acidic and moderately acidic conditions
275 was associated with changes mainly in NH_3 and sulfate levels. Days when pH reached almost 4, were characterized
276 by high K^+ in combination with high OA and EC levels and low sulfates suggesting significant influence of
277 biomass burning. At LAP the pH of $PM_{2.5}$ ranged from 2.72 to 3.41, with a mean value of 3.01 ± 0.31. Please note
278 that only 4 days of $PM_{2.5}$ measurements were available in LAP during January 2020. The fine aerosol in IOA had
279 the lowest overall acidity with a mean value of 4.08 ± 0.42 units and a range between 3.55 and 5.14 units. These
280 levels of acidity are a consequence of the intense biomass burning during this winter campaign at IOA (Kaskaoutis
281 et al., 2022). Elevated K^+ levels were observed, due almost entirely to wood burning for heating. Comparing IOA
282 with the other sites in January, there is a statistically significant difference in aerosol acidity levels due to higher
283 Ca^{2+}, K^+ and NH_3 combined with lower temperature, despite the high sulfates levels in the area (Table 1). At PTR
284 aerosol pH ranged from 2.82 to 4.44 units with a mean value of 3.70 ± 0.45. NVCs (Ca^{2+}, K^+, Mg^{2+} and Na^+), NH_3
285 and sulfates drove the variability of the aerosol pH most of the days. Aerosols at LAP and XAN exhibited the
286 highest acidity (lowest pH levels) among all studied sites, while IOA and PTR exhibited the highest aerosol pH
287 levels (Fig. 3a). Remarkably, aerosol acidity at the urban background site (THI) was similar to that at the coastal
288 background site (FKL). On the other hand, the suburban site (PTR) had higher aerosol pH mainly due to the likely
289 higher NH_3 levels at PTR than THI and FKL (Table 1), considering though the different ways NH_3 was measured
290 for these sites. Considering the two remote rural and coastal areas (XAN and FKL), their fine aerosol pH differed
291 by about half a pH unit due to increased Na^+, Mg^{2+} and relative humidity levels at FKL together with slightly
292 higher sulfate concentrations at XAN.

293   The accuracy of the aerosol pH predictions using ISORROPIA-lite was evaluated by comparing the observed
294 with the predicted partitioning coefficient of NH_4^+ ($\varepsilon(NH_4^+)$) and this comparison was possible only at PTR during
295 winter when both NH_3 and NH_4^+ were measured. A useful way to assess the reliability and potential uncertainties
296 of such models' predictions of aerosol pH is the comparison between measured and simulated gas-particle
297 partitioning fractions of semivolatile species (Guo et al., 2016). Figure 4 shows the comparison of the observed
298 and predicted $\varepsilon(NH_4^+)$ calculated for the case of PTR in winter. We focus on PTR since it was the only site where
299 NH_3 in-situ measurements were available making it a more suitable case for such comparison. The measurements
300 and predictions of total NH_3 are well correlated ($R^2=0.78$) although the model underestimates by 30% the $\varepsilon(NH_4^+)$.
301 A sensitivity test and a re-evaluation of the model discussed in the supplementary section S4 (Fig S3) indicates
302 that this small underestimation can be attributed to the uncertainty in the HNO_3 levels. Sensitivity tests regarding
303 the gas phase NH_3 and HNO_3 used to estimate aerosol pH are also provided (section 3.4). Overall, $PM_{2.5}$ during
304 winter varied acidic to moderately acidic with an average pH across all studied urban and urban background sites
305 of 3.57 ± 0.44. The overall $PM_{2.5}$ pH range across all 6 sites was from 1.72 to 5.14.

3.2.2 Summer

The seasonal variation of the acidity of PM$_{2.5}$ was investigated at three of the sites, THI, FKL and IOA in which measurements were available for the summer 2019 PANACEA campaign. The mean PM$_{2.5}$ composition is summarized in Table 1. During the whole period, PM$_{2.5}$ at the three sites was acidic with a mean pH of 1.35 ± 0.18 at THI, 1.75 ± 0.62 at IOA and 2.08 ± 0.45 pH at FKL (Figure 3c). At THI the PM$_{2.5}$ pH was consistently low throughout the summer period with a minimum value of 1.13, and a maximum of 2. At IOA and FKL the PM$_{2.5}$ pH was slightly higher than at THI. At FKL relative humidity levels increased the aerosol water content and together with the relatively high K$^+$ and Na$^+$ levels led to higher aerosol pH. Higher Ca^{2+} and K$^+$ levels at IOA and slightly higher sulfate levels at THI seemed to be the factors controlling the difference in the aerosol pH between these two sites. Overall, comparing the summertime (July and August) aerosol pH levels at the three sites (Fig. 3c and S5), a uniformity can be observed with high aerosol acidity being the case on most of the days, dropping even below 0 at IOA as a result of increased temperature and sulfate levels and reduced aerosol water. FKL and IOA had similar aerosol pH levels since most of the major aerosol components had similar concentrations at the two sites. The higher Ca^{2+} at IOA was balanced by the higher Na$^+$ in FKL.

3.2.3 Impact of organics

In order to investigate the potential effect of OA on the aerosol pH levels, ISORROPIA-lite was also run considering only the inorganic components of the aerosol (i.e. setting the OA concentration to zero). The mean difference between the aerosol pH calculated considering all aerosol components, including organics and the one accounting only for the inorganic content of PM$_{2.5}$ is shown in Figs. 3b and d for January 2020 and summer 2019, respectively. The water associated with the OA in most cases reduces the H$^+$ concentration and therefore increases the aerosol pH (Kakavas et al., 2022). However, this expected increase in aerosol pH due to OA was not always found at all sites, because of the resulting changes in the partitioning of the semivolatile compounds from the gas phase to the aerosol phase. This partitioning affects the OA induced change in the H$^+$ concentration (H$^+_{air}$ concentration in eq. 1), which together with aerosol water determine the aerosol pH.

In January at IOA, THI and PTR, the addition of aerosol water associated with the OA did not always increase the overall aerosol pH. In fact, a mean decrease of about 0.3 pH units was found at IOA, which had the highest OA concentrations among the 3 sites. Figure 5a depicts the aerosol water associated only with the inorganics along with the total one (i.e. including the OA water) and relative humidity and in Fig 5b the timeseries of the aerosol pH at IOA is shown in which again the one associated only with the inorganics and the one including the OA water (total aerosol pH) is depicted. An increase in the aerosol pH as a result of the addition of the organics is clear only at the end of January (from 26-01 to 29-01); the total aerosol pH was higher than the one when OA was absent (by 0.19 pH units on average). This was due to the high aerosol water content, which resulted from high relative humidity (above 80%). The addition of the OA increased aerosol water even more (Fig 5a). On all the other days in January with lower relative humidity, the addition of OA resulted in relative small increases in aerosol water. The partitioning of the semivolatile species to the aerosol phase increased, by decreasing the gas phase concentration (change up to 0.10 μg/m^3 for NH$_3$, 0.18 for HNO$_3$ and 0.12 for HCL), and similarly increasing the corresponding aerosol phase (NH$_4^+$, NO$_3^-$ and Cl$^-$). Furthermore, addition of considerable amounts of aerosol

water affects the activity coefficients of all ionic species (especially sulfate/bisulfate ions and NH_4^+), which shifts the ionic balance slightly. In addition, the free H^+ approximation of pH that we are using (eq.1) does not consider shifts in the activity coefficient in H^+ (Pye et al., 2020). Overall, the increase in the concentrations of the acids exceeded that of ammonium, therefore the concentration of H^+ increased. The increase in aerosol water did not counterbalance the increase in H^+ concentration resulting in a more acidic aerosol (lower aerosol pH). The highest decreases in pH were observed in days where high aerosol pH occurred (inorganic aerosol pH above 4.5 units, mean pH decrease 0.58 units). At the other two sites the aerosol pH decreased by about 0.08 pH units at THI and 0.01 at PTR. These relatively rare, but still important, set of conditions require further tests of thermodynamic model pH predictions.

At FKL, XAN and LAP a small increase in aerosol pH was found; 0.001, 0.05, 0.05 pH units increase respectively. In the summer (July and August), the pH increased at all sites when considering OA water, with the highest predicted increase of about 0.15 at IOA. At the other sites the aerosol pH increased by about 0.09 units at FKL and 0.11 at THI. Therefore, the effect of the organics on the pH at all sites was on average less than 0.3 units.

3.2.4 Main factors controlling seasonality of pH

A clear seasonal difference in acidity was observed at all sites. In summer $PM_{2.5}$ at FKL was 1 pH unit more acidic than in winter. To determine the main drivers of aerosol pH seasonal variability, a series of sensitivity simulations were performed using the concentrations of aerosol components and meteorological conditions observed in winter and replacing each time one of them by its corresponding mean value in summer. Then, the difference in the estimated aerosol pH was calculated. The factors that were tested were: temperature, relative humidity, TNO_3 (sum of gas-phase HNO_3 and particulate NO_3^-), TNH_3 (sum of gas-phase NH_3 and particulate NH_4^+), sulfates, Na^+, K^+, Ca^{2+} and OA. The results for FKL are shown in Fig. 6f and Table S5 as ΔpH, that is the pH of the base case simulation minus that of the perturbation scenario. Sulfate was the main contributor to the change in aerosol acidity between summer and winter at FKL, where the 2 $\mu g\ m^{-3}$ concentration difference between the two seasons resulted in 1.66 units of pH difference. Total NH_3 availability was the second most important factor with a mean ΔpH of 0.39 followed by temperature (mean ΔpH =0.30) and Na^+ (mean ΔpH =0.25). The effect of the remaining factors was on average less than 0.20 pH units; TNO_3 (mean ΔpH = 0.17), relative humidity (mean ΔpH = 0.16), K^+ (mean ΔpH = 0.15), Ca^{2+} (mean ΔpH = 0.14) and OA (mean ΔpH = 0.08).

At IOA, aerosol average pH levels differed by 2.26 pH units between summer and winter with higher aerosol pH in winter (Fig. 6a). Simulations were performed using ISORROPIA-lite for nine factors: temperature, relative humidity, TNO_3 (sum of gas-phase HNO_3 and particulate NO_3^-), TNH_3, SO_4^{2-}, Na^+, K^+, Ca^{2+} and OA. The results are shown in Fig. 6b and Table S6. The availability of total HNO_3 (ΔpH=0.98), temperature (ΔpH=0.76) and the total NH_3 (ΔpH=0.59) had the greatest influence on the seasonal aerosol pH difference. The effect of K^+ (ΔpH=0.53), sulfates (ΔpH=0.45) and Ca^{2+} (ΔpH=0.43), followed by organics (0.22), RH (0.21) and Na^+ (0.06) were also notable. High concentrations of K+ affecting the aerosol pH are associated with biomass burning as discussed in Kaskaoutis et al., (2022).

THI also exhibited a significant seasonal difference in the aerosol acidity with $PM_{2.5}$ being approximately 2.6 times more acidic in summer than in winter (Fig. 6c). Nine sensitivity tests were conducted for the effect of the nine factors tested for the other two sites on pH (Table S7, Fig. 6d). Sulfate was found to be the main contributor

414 to the more acidic conditions in summer at THI with a mean absolute difference in pH (winter - summer), ΔpH,
415 of 2.8 units, followed by TNH$_3$ and temperature with absolute ΔpH of 0.48 and 0.42 units, respectively. The other
416 factors contributed less to the seasonal difference in aerosol pH, with an absolute ΔpH varying between 0.10 and
417 0.33 units.

418

419 3.3 Aerosol water

420 ISORROPIA-lite can also be used to calculate the contribution of each inorganic salt and organic fraction to the
421 total aerosol water content. Fig. 7 depicts the average contributions of the various inorganic salts and of OA to the
422 total aerosol water for all sites in winter (January) (Fig. 7a) and summer (July and August) (Fig. 7b).

423   In January (Fig. 7a), OA contributed 60% to the total aerosol water at IOA and 55% at PTR. These were the
424 two sites with the highest levels of OA mainly due to residential wood burning. At LAP and THI, OA was also
425 the dominant aerosol component contributing to total aerosol water 37% and 33% respectively, while at XAN
426 sulfate salts were associated with 42% and OA with 32% of the water. Focusing on the inorganic components
427 alone, aerosol water was found to be controlled by nitrate and sulfate. Nitrate had the highest contributions to
428 inorganic aerosol water at IOA (24%), THI (31%), LAP (30%) and PTR (21%). NH$_4$NO$_3$ was the dominant salt
429 at IOA, LAP and PTR; while at THI NaNO$_3$ contributed 25% to the total water associated with inorganics along
430 with NH$_4$NO$_3$ (22%). The situation at FKL was different with chloride and sulfate being the major contributors to
431 aerosol water (40% and 36% respectively), while OA had only a minor contribution (5%) due to its very low
432 concentration at this site. The dominant chloride salt at FKL was NH$_4$Cl contributing 31% to the total inorganic
433 water while Na$_2$SO$_4$ was the major sulfate salt, contributing 17%.

434   In July and August in the three sites with available observations, sulfate dominated aerosol water (Fig. 7b)
435 with contributions ranging from 70% at IOA to 80% at FKL and THI. (NH$_4$)$_2$SO$_4$ was the dominant salt at all
436 three sites, contributing more than half of the total water content at THI (58%) and 38% and 40% at IOA and
437 FKL, respectively. The second most dominant aerosol component was OA with 19% contribution to the total
438 aerosol water at THI, 27% at IOA and 14% at FKL.

439

440 3.4 Sensitivity of pH to NH$_3$ and HNO$_3$

441 Studies with ISORROPIA-II (Guo et al., 2015, Weber et al., 2016) have shown that neglecting gas-phase NH$_3$ in
442 the thermodynamic equilibrium calculation of pH results in an underestimation of at most one pH unit (Bougiatioti
443 et al., 2016). Due to the lack of in situ measurements of the gas phase NH$_3$ (except PTR) and HNO$_3$ during the
444 campaign periods, a sensitivity test was conducted varying the assumed concentrations of the gases that we used
445 for the aerosol pH estimation. In detail, simulations with half and double the concentrations of NH$_3$ and HNO$_3$
446 were conducted for all sites during both periods; winter (January) and summer (July and August). The resulted
447 difference in aerosol pH (ΔpH) due to these altered gas phase concentrations are depicted in Fig. 8 and the mean
448 values of ΔpH for each simulation are summarized in Table S8 along with the concentrations of the gases for the
449 base case scenarios (i.e. the concentrations used for the main simulations). For the case of NH$_3$, an average (across
450 all sites and both periods) of 0.25 increase in aerosol pH was observed when double the amount of NH$_3$ introduced
451 to each system and the increase in pH ranged between 0.13 and 0.34 pH units. On the other hand, when half the
452 amount of NH$_3$ was used a smaller change was observed across the sites; the mean decrease in aerosol pH was -

453 0.19 pH units while it ranged from -0.07 to -0.31 units. For the sensitivity simulations varying the amount of
454 HNO$_3$ the overall change in aerosol pH was much less distinct. The mean decrease in the pH of the aerosol was
455 between 0.01 and 0.15 pH units when the concentration of HNO$_3$ was doubled (the overall mean decrease was
456 0.06). Using half the concentration of HNO$_3$ resulted in a mean increase ranging from 0.01 to 0.15 pH units.
457 According to this sensitivity analysis, the uncertainty in the gas phase NH$_3$ could explain about half of the seasonal
458 difference in aerosol pH that was presented and discussed in section 3.2.4 about the factors affecting the
459 seasonality of pH. The uncertainty in gas phase NH$_3$ could explain a larger fraction of the seasonal difference in
460 aerosol pH in IOA than in FKL and THI, which is expected since at these two sites aerosol pH seasonality was
461 predominately driven by sulfates. Our results show a factor of 2 uncertainty in NH$_3$ lead to an average pH
462 difference of 0.25 units that has minor impact on our findings discussed below.

463

464 3.5.1 Sensitivity of PM levels to NH$_3$ and HNO$_3$ availability

465 We used the framework developed by Nenes et al. (2020) that relates the levels of aerosol pH with the formation
466 of aerosol nitrate (and ammonium), to investigate the sensitivity of the different aerosol systems studied here to
467 the gas-phase concentrations of NH$_3$ and HNO$_3$. The main parameters used in this framework that control the
468 secondary inorganic particulate matter sensitivity are the aerosol pH, liquid water content and temperature. The
469 conceptual idea is that there is a "sensitivity window" of pH levels in which the partitioning of nitrate shifts from
470 nitrate being predominately gaseous to mostly in the aerosol phase. When acidity is below this pH sensitivity
471 window, particulate nitrate is almost non-existent and consequently aerosol levels are insensitive to HNO$_3$
472 availability. In this case, aerosol reduction policies that only target HNO$_3$ reduction cannot be effective (Nenes et
473 al., 2020), as there is no nitrate in the aerosol phase. Based on these criteria, this framework defines characteristic
474 levels of aerosol acidity at which the aerosol becomes insensitive to NH$_3$ (or HNO$_3$) levels and vice versa.
475 Therefore, four possible regimes of PM sensitivity can be derived; i) neither NH$_3$ nor HNO$_3$ are important for PM
476 formation, or PM formation is dominated by ii) HNO$_3$, iii) both NH$_3$ and HNO$_3$, and iv) NH$_3$ alone.

477 Figure 9 shows the PM$_{2.5}$ sensitivity maps derived using this framework and the daily data at all stations in
478 January 2020 (Fig. 9a) and at FKL, THI and IOA in summer (July and August) (Fig. 9b) (34 days in total; in July
479 and August 2019). Considering the average temperature across the 3 sites (Table S9) the pH sensitivity window
480 for each of the two gases (NH$_3$ and HNO$_3$) was calculated as a function of aerosol water (LWC). The data that
481 were used as well as the aerosol pH and water from the combination of the datasets from the 3 sites are given in
482 Table S9.

483 During January, an overall sensitivity of PM$_{2.5}$ to HNO$_3$ is found as most of the points of the sites reside above
484 the blue line thus an increase in HNO$_3$ concentration will lead to its partitioning to the aerosol phase as nitrate.
485 On the other hand, most points are also above the red line indicating that PM$_{2.5}$ is relatively insensitive to gas
486 phase NH$_3$. Depending on the conditions and aerosol acidity levels, each site may have some days that deviate
487 from the HNO$_3$-only sensitivity region. At FKL out of the 17 days where HNO$_3$ sensitivity dominated, on 4 days
488 PM$_{2.5}$ was sensitive to both HNO$_3$ and NH$_3$ levels due to the slightly more acidic particles present. At THI PM$_{2.5}$
489 was sensitive to HNO$_3$ on all 27 days that were examined, except for two days in which NH$_3$ sensitivity regime
490 also occurred and characterized by lower aerosol pH values (2.05 and 2.13 pH units). At IOA as a consequence
491 of the lower aerosol acidity, PM$_{2.5}$ was (as expected) almost exclusively in the HNO$_3$ sensitive regime where NH$_3$

492 mass variations would not affect PM concentration. At IOA, NH_3 availability was found to play a role in aerosol
493 formation in two days when the aerosol water was very high in combination with the aerosol pH being slightly
494 lower. Regions with more acidic particles i.e. XAN and LAP were also in some cases in the HNO_3 and NH_3
495 sensitive region.

496 During summer (July and August) $PM_{2.5}$ shifted out of the HNO_3 only sensitive region at all three sites and
497 NH_3 started to play a more important role for the aerosol levels due to the more acidic conditions compared to
498 January. In many days at IOA and some at FKL the sensitivity to HNO_3 and the insensitive regime also seemed
499 to exist when extremely low aerosol water content was present. At THI $PM_{2.5}$ sensitivity showed the least
500 "dispersed" picture compared to the other sites, and $PM_{2.5}$ was exclusively sensitive to NH_3 availability due to the
501 consistently high aerosol acidity conditions. Consequently, for the studied period the inorganic $PM_{2.5}$ levels at
502 THI in winter would be reduced by limitation of HNO_3 formation, which depends on VOC and NO_x conditions,
503 and NH_3 controls in summer. However, sulfate is the major inorganic $PM_{2.5}$ component during the summer so the
504 NH_3 reductions would have a relatively small effect on the total fine PM. The inclusion of the OA in the aerosol
505 pH and water calculations resulted in a small difference in terms of these sensitivity maps. As the aerosol water
506 increased slightly, in a few cases in XAN the PM sensitivity was shifted from insensitive to HNO_3 sensitive, while
507 in a few cases in IOA and FKL, PM also became sensitive to NH_3 (Fig. S6).

508

509 3.5.2 Importance of semivolatiles for deposition

510 Aerosol acidity and water effects on the partitioning of HNO_3 and NH_3 are linked with the total deposition of these
511 species, in both their gas and particulate forms. As HNO_3 and NH_3 are deposited about 10 times faster than their
512 particulate forms (NO_3^-, NH_4^+), the partitioning between gas and particulate phase affects how fast HNO_3/ NO_3^-
513 or NH_3/ NH_4^+ are deposited (Nenes et al., 2021) and therefore the distance to which they are transported within
514 the atmosphere before deposition (Baker et al., 2021). This gas-to-particle partitioning depends on the pH of the
515 aerosol water and on the LWC of the aerosol (Guo et al., 2015). Therefore, "fast" and "slow" deposition regimes
516 for HNO_3 and NH_3 can be defined as a function of aerosol pH and LWC. Figure 10 shows the reactive nitrogen
517 (sum of TNO_3 and TNH_3) deposition regimes at the sites, where data were available both in January (Fig. 10a)
518 and summer (July and August) (Fig. 10b), calculated using the average temperatures of the datasets for each
519 season. Looking at the characterization of the deposition domains for all the studied sites during January, a main
520 difference can be observed in terms of the nitrogen deposition velocity (Fig. 10a). At all sites, NH_3 seems to
521 always experience fast deposition. On the other hand, nitrate's deposition rate varies between fast (as gaseous
522 HNO_3) and slow (as particulate NO_3^-), leading to local removal or long-range transport, respectively. IOA and
523 PTR cases are almost exclusively in the HNO_3 slow – NH_3 fast regime due to the higher aerosol pH levels that
524 enhance HNO_3 partitioning to the particulate phase. The other sites are characterized by high deposition rates for
525 both NH_3 and HNO_3. In summer, the deposition is similarly characterized as fast for both NH_3 and HNO_3 at FKL,
526 THI and IOA due to the higher acidity levels. The higher temperature in summer than in winter also favors the
527 fast removal of both HNO_3 and NH_3, with the exception of one day at IOA characterized by extremely low aerosol
528 pH (below zero), where NH_3 was present in the form of particulate NH_4^+ and thus had a slow deposition velocity.
529 Including the OA in the calculations did not change as much the deposition rates (Fig. S7). In a few cases during
530 January in THI and PTR the deposition rate of HNO_3 shifted from fast to slow due to the addition of OA water.

531

Conclusions

This study was based on PM$_{2.5}$ chemical composition observations in 6 regions of Greece (Finokalia, FKL; Thissio, THI; Patras, PTR; Ioannina, IOA; Xanthi, XAN; and Thessaloniki, LAP) during summer 2019 (in FKL, THI and IOA) and winter 2019-2020 (in all regions) as part of the national research infrastructure PANACEA. The aerosol composition measurements together with the gas phase NH$_3$, HNO$_3$ data were used in the thermodynamic model ISORROPIA-lite to calculate the fine aerosol pH at all the sites and to determine its seasonal variation.

The pH levels of PM$_{2.5}$ across Greece during winter ranged from 1.72 to 5.14. The highest pH values were estimated at IOA (4.08 ± 0.42) and PTR (3.70 ± 0.45) followed by THI (3.30 ± 0.48) and FKL (3.25 ± 0.37), while aerosols at XAN and LAP were the most acidic (2.81 ± 0.53 and 3.01 ± 0.31, respectively). The lowest acidity at IOA was associated with high K$^+$ levels from biomass burning emissions in combination with high Ca^{2+} and NH$_3$ and low temperatures. Similar factors (NH$_3$ and cation levels) affected PTR aerosol pH. The aerosol acidity levels at the urban background site (THI) were similar to those at the coastal background site (FKL). High nonvolatile cation concentrations at FKL, together with elevated humidity levels resulted in a higher mean aerosol pH compared to the rural background site (XAN), which had slightly higher levels of sulfates than FKL.

In summer, PM$_{2.5}$ was generally more acidic than in winter at the three sites studied (THI, IOA and FKL), with mean pH values of 1.35 ± 0.18 (THI), 1.75 ± 0.62 (IOA) and 2.08 ± 0.45 units (FKL). pH in summer was lower than winter by 1 (FKL) to about 2 (THI and IOA) pH units. Sulfates drive the seasonal variation in aerosol pH at THI and FKL. At IOA, on the other hand, temperature together with NH$_3$ and HNO$_3$ availability were the main drivers of the seasonal difference in aerosol acidity, with K$^+$, Ca^{2+}, and sulfates also contributing.

Organics contributed significantly to the total fine aerosol mass at all sites but FKL in January. OA was found to be the main contributor to the total aerosol water at IOA and PTR (60% and 55% contribution, respectively) due to the OA levels in these sites, and the dominant contributor at THI and LAP (33% and 37% contribution respectively). During January nitrate salts contributed more to the total aerosol water at IOA (24%), THI (31%), LAP (30%) and PTR (21%), with NH$_4$NO$_3$ being the dominant salt present at IOA, LAP and PTR and NaNO$_3$ at THI. The aerosol water content at XAN was dominated by sulfate (42%), with OA also contributing to the total aerosol water (32%). Chloride and sulfate contributed more to the aerosol water at FKL (40% and 36% respectively). During summer (July and August), sulfate salts contributed more to LWC at all sites (80% contribution at FKL and THI and 70% at IOA), with (NH$_4$)$_2$SO$_4$ being the dominant species of the inorganic LWC at all three sites. At sites with higher aerosol pH (IOA, THI and PTR in January), the water associated with the organics did not increase aerosol pH in most cases. This behavior associated with aerosol pH above 4 units is the result of increased partitioning of semivolatiles to the aerosol phase and of changes in the activity coefficients. Such conditions are good benchmark for testing the thermodynamic model predictions of pH.

PM$_{2.5}$ mass was sensitive to the availability of total HNO$_3$ at all sites during January 2020. At LAP and XAN, PM mass was also found to be sensitive to NH$_3$. In summer (July and August), PM at all three sites examined showed a strong sensitivity to NH$_3$ due to the low summertime aerosol pH. In some cases, the PM$_{2.5}$ concentrations at FKL and IOA appeared insensitive to both precursor species due to the low water content of the aerosols. PM sensitivity at THI in summer showed a clear dependence on NH$_3$, reflecting the higher summertime aerosol

acidity. Our results show that HNO_3 levels (could contribute to) regulate $PM_{2.5}$ mass concentration which however was mainly composed by OA and sulfate, hence policies targeted to reduce $PM_{2.5}$ levels in Greece would be more effective by reducing HNO_3 levels (i.e. transportation sector) in addition to OA and sulfate.

Finally, our analysis has shown that in Greece NH_3 deposition is fast, whereas deposition of HNO_3/NO_3^- may occur locally near the sources or remotely by long-range transport, depending on the environmental conditions. How future changes in the meteorological conditions and in air pollutant emissions will affect the aerosol pH and the factors controlling it, as well as atmospheric residence time and deposition of reactive nitrogen in the region, requires further investigation.

Acknowledgements. We acknowledge support of this work by the project "PANhellenic infrastructure for Atmospheric Composition and climatE change" (MIS 5021516) which is implemented under the Action "Reinforcement of the Research and Innovation Infrastructure", funded by the Operational Programme "Competitiveness, Entrepreneurship and Innovation" (NSRF 2014-2020) and co-financed by Greece and the European Union (European Regional Development Fund), by the European Research Council (ERC-2016-COG), Project Pyrogenic TRansformations Affecting Climate and Health (PyroTRACH-726165) by the Horizon-2020 Project FORCeS of the European Union under grant agreement No 821205 and by the Horizon-2020 project Research Infrastructures Services Reinforcing Air Quality Monitoring Capacities in European Urban & Industrial AreaS (RI-URBANS) grant agreement No. 101036245.

Colorblind friendly palettes were used to create the figures according to and described in (Crameri et al., 2020). More information about the abovementioned palettes can be found in https://doi.org/10.5281/zenodo.8409685 (Crameri, 2018).

Code availability. ISORROPIA-lite is openly available at https://www.epfl.ch/labs/lapi/models-and-software/isorropia/

Data availability. Observational data are available upon request by the corresponding site principal investigator.

Competing interests. Some authors are members of the editorial board of journal Atmospheric Chemistry and Physics

Author contributions. AMN collected the data, performed the simulations and wrote the manuscript, MK conceived the study and supervised the work. MK and SP edited the manuscript, AN provided the thermodynamic codes and sensitivity/deposition routines for analysis of the data, and advised on their application/interpretation. MT, EL, KP, KT, IT, CK, FB, AK, KM, GK, NK, NH provided data; all authors provided comments on the manuscript.

607 **References**

608

609 Baker, A. R., Kanakidou, M., Nenes, A., Myriokefalitakis, S., Croot, P. L., Duce, R. A., Gao, Y., Guieu, C., Ito,
610 A., Jickells, T. D., Mahowald, N. M., Middag, R., Perron, M. M. G., Sarin, M. M., Shelley, R., and Turner, D.
611 R.: Changing atmospheric acidity as a modulator of nutrient deposition and ocean biogeochemistry, Sci. Adv., 7,
612 eabd8800, https://doi.org/10.1126/sciadv.abd8800, 2021.

613 Bougiatioti, A., Fountoukis, C., Kalivitis, N., Pandis, S. N., Nenes, A., and Mihalopoulos, N.: Cloud
614 condensation nuclei measurements in the marine boundary layer of the Eastern Mediterranean: CCN closure and
615 droplet growth kinetics, Atmos. Chem. Phys., 9, 7053–7066, https://doi.org/10.5194/acp-9-7053-2009, 2009.

616 Bougiatioti, A., Nikolaou, P., Stavroulas, I., Kouvarakis, G., Weber, R., Nenes, A., Kanakidou, M., and
617 Mihalopoulos, N.: Particle water and pH in the eastern Mediterranean: source variability and implications for
618 nutrient availability, Atmos. Chem. Phys., 16, 4579–4591, https://doi.org/10.5194/acp-16-4579-2016, 2016.

619 Clegg, S. L., Seinfeld, J. H., and Brimblecombe, P.: Thermodynamic modelling of aqueous aerosols containing
620 electrolytes and dissolved organic compounds, Journal of Aerosol Science, 32, 713–738,
621 https://doi.org/10.1016/S0021-8502(00)00105-1, 2001.

622 Crameri, F.: Geodynamic diagnostics, scientific visualisation and StagLab 3.0, https://doi.org/10.5194/gmd-
623 2017-328, 20 February 2018.

624 Crameri, F., Shephard, G. E., and Heron, P. J.: The misuse of colour in science communication, Nat Commun,
625 11, https://doi.org/10.1038/s41467-020-19160-7, 2020.

626 Ding, J., Zhao, P., Su, J., Dong, Q., Du, X., and Zhang, Y.: Aerosol pH and its driving factors in Beijing, Atmos.
627 Chem. Phys., 19, 7939–7954, https://doi.org/10.5194/acp-19-7939-2019, 2019.

628 Fang, T., Guo, H., Zeng, L., Verma, V., Nenes, A., and Weber, R. J.: Highly Acidic Ambient Particles, Soluble
629 Metals, and Oxidative Potential: A Link between Sulfate and Aerosol Toxicity, Environ. Sci. Technol., 51,
630 2611–2620, https://doi.org/10.1021/acs.est.6b06151, 2017.

631 Flocas, H., Kelessis, A., Helmis, C., Petrakakis, M., Zoumakis, M., and Pappas, K.: Synoptic and local scale
632 atmospheric circulation associated with air pollution episodes in an urban Mediterranean area, Theor Appl
633 Climatol, 95, 265–277, https://doi.org/10.1007/s00704-008-0005-9, 2009.

634 Florou, K., Papanastasiou, D. K., Pikridas, M., Kaltsonoudis, C., Louvaris, E., Gkatzelis, G. I., Patoulias, D.,
635 Mihalopoulos, N., and Pandis, S. N.: The contribution of wood burning and other pollution sources to
636 wintertime organic aerosol levels in two Greek cities, Atmos. Chem. Phys., 17, 3145–3163,
637 https://doi.org/10.5194/acp-17-3145-2017, 2017.

638 Fountoukis, C. and Nenes, A.: ISORROPIA II: a computationally efficient thermodynamic equilibrium model
639 for K+–Ca2+–Mg2+–NH+4 –Na+–SO24−–NO−3 –Cl−–H2O aerosols, Atmos. Chem. Phys., 21, 2007.

640 Guo, H., Xu, L., Bougiatioti, A., Cerully, K. M., Capps, S. L., Hite, J. R., Carlton, A. G., Lee, S.-H., Bergin, M.
641 H., Ng, N. L., Nenes, A., and Weber, R. J.: Fine-particle water and pH in the southeastern United States, Atmos.
642 Chem. Phys., 15, 5211–5228, https://doi.org/10.5194/acp-15-5211-2015, 2015.

643 Guo, H., Sullivan, A. P., Campuzano-Jost, P., Schroder, J. C., Lopez-Hilfiker, F. D., Dibb, J. E., Jimenez, J. L.,
644 Thornton, J. A., Brown, S. S., Nenes, A., and Weber, R. J.: Fine particle pH and the partitioning of nitric acid
645 during winter in the northeastern United States, J. Geophys. Res. Atmos., 121,
646 https://doi.org/10.1002/2016JD025311, 2016.

647 Guo, H., Liu, J., Froyd, K. D., Roberts, J. M., Veres, P. R., Hayes, P. L., Jimenez, J. L., Nenes, A., and Weber,
648 R. J.: Fine particle pH and gas–particle phase partitioning of inorganic species in Pasadena, California, during
649 the 2010 CalNex campaign, Atmos. Chem. Phys., 17, 5703–5719, https://doi.org/10.5194/acp-17-5703-2017,
650 2017a.

Guo, H., Weber, R. J., and Nenes, A.: High levels of ammonia do not raise fine particle pH sufficiently to yield nitrogen oxide-dominated sulfate production, Sci Rep, 7, 12109, https://doi.org/10.1038/s41598-017-11704-0, 2017b.

Guo, H., Otjes, R., Schlag, P., Kiendler-Scharr, A., Nenes, A., and Weber, R. J.: Effectiveness of ammonia reduction on control of fine particle nitrate, Atmos. Chem. Phys., 18, 12241–12256, https://doi.org/10.5194/acp-18-12241-2018, 2018.

Hildebrandt, L., Kostenidou, E., Lanz, V. A., Prevot, A. S. H., Baltensperger, U., Mihalopoulos, N., Laaksonen, A., Donahue, N. M., and Pandis, S. N.: Sources and atmospheric processing of organic aerosol in the Mediterranean: insights from aerosol mass spectrometer factor analysis, Atmos. Chem. Phys., 11, 12499–12515, https://doi.org/10.5194/acp-11-12499-2011, 2011.

Kakavas, S., Patoulias, D., Zakoura, M., Nenes, A., and Pandis, S. N.: Size-resolved aerosol pH over Europe during summer, Atmos. Chem. Phys., 21, 799–811, https://doi.org/10.5194/acp-21-799-2021, 2021.

Kakavas, S., Pandis, S. N., and Nenes, A.: ISORROPIA-Lite: A Comprehensive Atmospheric Aerosol Thermodynamics Module for Earth System Models, Tellus B: Chemical and Physical Meteorology, 74, 1–23, https://doi.org/10.16993/tellusb.33, 2022.

Kalkavouras, P., Bougiatioti, A., Kalivitis, N., Stavroulas, I., Tombrou, M., Nenes, A., and Mihalopoulos, N.: Regional new particle formation as modulators of cloud condensation nuclei and cloud droplet number in the eastern Mediterranean, Atmos. Chem. Phys., 19, 6185–6203, https://doi.org/10.5194/acp-19-6185-2019, 2019.

Kanakidou, M., Myriokefalitakis, S., and Tsigaridis, K.: Aerosols in atmospheric chemistry and biogeochemical cycles of nutrients, Environ. Res. Lett., 13, 063004, https://doi.org/10.1088/1748-9326/aabcdb, 2018.

Kaskaoutis, D. G., Grivas, G., Theodosi, C., Tsagkaraki, M., Paraskevopoulou, D., Stavroulas, I., Liakakou, E., Gkikas, A., Hatzianastassiou, N., Wu, C., Gerasopoulos, E., and Mihalopoulos, N.: Carbonaceous Aerosols in Contrasting Atmospheric Environments in Greek Cities: Evaluation of the EC-tracer Methods for Secondary Organic Carbon Estimation, Atmosphere, 11, 161, https://doi.org/10.3390/atmos11020161, 2020.

Kaskaoutis, D. G., Grivas, G., Oikonomou, K., Tavernaraki, P., Papoutsidaki, K., Tsagkaraki, M., Stavroulas, I., Zarmpas, P., Paraskevopoulou, D., Bougiatioti, A., Liakakou, E., Gavrouzou, M., Dumka, U. C., Hatzianastassiou, N., Sciare, J., Gerasopoulos, E., and Mihalopoulos, N.: Impacts of severe residential wood burning on atmospheric processing, water-soluble organic aerosol and light absorption, in an inland city of Southeastern Europe, Atmospheric Environment, 280, 119139, https://doi.org/10.1016/j.atmosenv.2022.119139, 2022.

Kastelis, N. and Kourtidis, K.: Characteristics of the atmospheric electric field and correlation with CO2 at a rural site in southern Balkans, Earth Planet Sp, 68, 3, https://doi.org/10.1186/s40623-016-0379-3, 2016.

Kostenidou, E., Florou, K., Kaltsonoudis, C., Tsiflikiotou, M., Vratolis, S., Eleftheriadis, K., and Pandis, S. N.: Sources and chemical characterization of organic aerosol during the summer in the eastern Mediterranean, Atmos. Chem. Phys., 15, 11355–11371, https://doi.org/10.5194/acp-15-11355-2015, 2015.

Lemou, A., Rabhi, L., Merabet, H., Ladji, R., Nicolas, J. B., Bonnaire, N., Mustapha, M. A., Dilmi, R., Sciare, J., Mihalopoulos, N., and Yassaa, N.: Chemical characterization of fine particles (PM2.5) at a coastal site in the South Western Mediterranean during the ChArMex experiment, Environ Sci Pollut Res, 27, 20427–20445, https://doi.org/10.1007/s11356-020-08168-7, 2020.

Liakakou, E., Fourtziou, L., Paraskevopoulou, D., Speyer, O., Lianou, M., Grivas, G., Myriokefalitakis, S., and Mihalopoulos, N.: High-Resolution Measurements of SO2, HNO3 and HCl at the Urban Environment of Athens, Greece: Levels, Variability and Gas to Particle Partitioning, Atmosphere, 13, 218, https://doi.org/10.3390/atmos13020218, 2022.

Liu, M., Song, Y., Zhou, T., Xu, Z., Yan, C., Zheng, M., Wu, Z., Hu, M., Wu, Y., and Zhu, T.: Fine particle pH during severe haze episodes in northern China: Fine Particle pH During Haze Episodes, Geophys. Res. Lett., 44, 5213–5221, https://doi.org/10.1002/2017GL073210, 2017.

Masiol, M., Squizzato, S., Formenton, G., Khan, M. B., Hopke, P. K., Nenes, A., Pandis, S. N., Tositti, L., Benetello, F., Visin, F., and Pavoni, B.: Hybrid multiple-site mass closure and source apportionment of PM2.5 and aerosol acidity at major cities in the Po Valley, Science of The Total Environment, 704, 135287, https://doi.org/10.1016/j.scitotenv.2019.135287, 2020.

Mihalopoulos, N., Stephanou, E., Kanakidou, M., Pilitsidis, S., and Bousquet, P.: Tropospheric aerosol ionic composition in the Eastern Mediterranean region, Tellus B, 49, 314–326, https://doi.org/10.1034/j.1600-0889.49.issue3.7.x, 1997.

Nenes, A., Pandis, S. N., Weber, R. J., and Russell, A.: Aerosol pH and liquid water content determine when particulate matter is sensitive to ammonia and nitrate availability, Atmos. Chem. Phys., 20, 3249–3258, https://doi.org/10.5194/acp-20-3249-2020, 2020.

Nenes, A., Pandis, S. N., Kanakidou, M., Russell, A. G., Song, S., Vasilakos, P., and Weber, R. J.: Aerosol acidity and liquid water content regulate the dry deposition of inorganic reactive nitrogen, Atmos. Chem. Phys., 21, 6023–6033, https://doi.org/10.5194/acp-21-6023-2021, 2021.

Paglione, M., Decesari, S., Rinaldi, M., Tarozzi, L., Manarini, F., Gilardoni, S., Facchini, M. C., Fuzzi, S., Bacco, D., Trentini, A., Pandis, S. N., and Nenes, A.: Historical Changes in Seasonal Aerosol Acidity in the Po Valley (Italy) as Inferred from Fog Water and Aerosol Measurements, Environ. Sci. Technol., 55, 7307–7315, https://doi.org/10.1021/acs.est.1c00651, 2021.

Pikridas, M., Bougiatioti, A., Hildebrandt, L., Engelhart, G. J., Kostenidou, E., Mohr, C., Prévôt, A. S. H., Kouvarakis, G., Zarmpas, P., Burkhart, J. F., Lee, B.-H., Psichoudaki, M., Mihalopoulos, N., Pilinis, C., Stohl, A., Baltensperger, U., Kulmala, M., and Pandis, S. N.: The Finokalia Aerosol Measurement Experiment – 2008 (FAME-08): an overview, Atmos. Chem. Phys., 10, 6793–6806, https://doi.org/10.5194/acp-10-6793-2010, 2010.

Pikridas, M., Tasoglou, A., Florou, K., and Pandis, S. N.: Characterization of the origin of fine particulate matter in a medium size urban area in the Mediterranean, Atmospheric Environment, 80, 264–274, https://doi.org/10.1016/j.atmosenv.2013.07.070, 2013.

Powley, H. R., Cappellen, P. V., and Krom, M. D.: Nutrient Cycling in the Mediterranean Sea: The Key to Understanding How the Unique Marine Ecosystem Functions and Responds to Anthropogenic Pressures, in: Mediterranean Identities - Environment, Society, Culture, edited by: Fuerst-Bjelis, B., InTech, https://doi.org/10.5772/intechopen.70878, 2017.

Psichoudaki, M., Nenes, A., Florou, K., Kaltsonoudis, C., and Pandis, S. N.: Hygroscopic properties of atmospheric particles emitted during wintertime biomass burning episodes in Athens, Atmospheric Environment, 178, 66–72, https://doi.org/10.1016/j.atmosenv.2018.01.004, 2018.

Putaud, J.-P., Raes, F., Van Dingenen, R., Brüggemann, E., Facchini, M.-C., Decesari, S., Fuzzi, S., Gehrig, R., Hüglin, C., Laj, P., Lorbeer, G., Maenhaut, W., Mihalopoulos, N., Müller, K., Querol, X., Rodriguez, S., Schneider, J., Spindler, G., Brink, H. T., Tørseth, K., and Wiedensohler, A.: A European aerosol phenomenology—2: chemical characteristics of particulate matter at kerbside, urban, rural and background sites in Europe, Atmospheric Environment, 38, 2579–2595, https://doi.org/10.1016/j.atmosenv.2004.01.041, 2004.

Pye, H. O. T., Nenes, A., Alexander, B., Ault, A. P., Barth, M. C., Clegg, S. L., Collett, J. L., Fahey, K. M., Hennigan, C. J., Herrmann, H., Kanakidou, M., Kelly, J. T., Ku, I. T., Faye McNeill, V., Riemer, N., Schaefer, T., Shi, G., Tilgner, A., Walker, J. T., Wang, T., Weber, R., Xing, J., Zaveri, R. A., and Zuend, A.: The acidity of atmospheric particles and clouds, Atmospheric Chemistry and Physics, 20, 4809–4888, https://doi.org/10.5194/acp-20-4809-2020, 2020.

Sciare, J., Oikonomou, K., Favez, O., Liakakou, E., Markaki, Z., Cachier, H., and Mihalopoulos, N.: Long-term measurements of carbonaceous aerosols in the Eastern Mediterranean: evidence of long-range transport of biomass burning, Atmos. Chem. Phys., 2008.

Seinfeld, J. H. and Pandis, S. N.: Atmospheric chemistry and physics: from air pollution to climate change, 2nd ed., J. Wiley, Hoboken, N.J, 1203 pp., 2006.

Διαγράφηκε: a

Διαγράφηκε: Pye, H. O. T., Nenes, A., Alexander, B., Ault, A. P., Barth, M. C., Clegg, S. L., Collett Jr., J. L., Fahey, K. M., Hennigan, C. J., Herrmann, H., Kanakidou, M., Kelly, J. T., Ku, I.-T., McNeill, V. F., Riemer, N., Schaefer, T., Shi, G., Tilgner, A., Walker, J. T., Wang, T., Weber, R., Xing, J., Zaveri, R. A., and Zuend, A.: The acidity of atmospheric particles and clouds, Atmos. Chem. Phys., 20, 4809–4888, https://doi.org/10.5194/acp-20-4809-2020, 2020b.¶

Shephard, M. W. and Cady-Pereira, K. E.: Cross-track Infrared Sounder (CrIS) satellite observations of tropospheric ammonia, Atmos. Meas. Tech., 8, 1323–1336, https://doi.org/10.5194/amt-8-1323-2015, 2015.

Shephard, M. W., Dammers, E., Cady-Pereira, K. E., Kharol, S. K., Thompson, J., Gainariu-Matz, Y., Zhang, J., McLinden, C. A., Kovachik, A., Moran, M., Bittman, S., Sioris, C. E., Griffin, D., Alvarado, M. J., Lonsdale, C., Savic-Jovcic, V., and Zheng, Q.: Ammonia measurements from space with the Cross-track Infrared Sounder: characteristics and applications, Atmos. Chem. Phys., 20, 2277–2302, https://doi.org/10.5194/acp-20-2277-2020, 2020.

Shi, G., Xu, J., Peng, X., Xiao, Z., Chen, K., Tian, Y., Guan, X., Feng, Y., Yu, H., Nenes, A., and Russell, A. G.: pH of Aerosols in a Polluted Atmosphere: Source Contributions to Highly Acidic Aerosol, Environ. Sci. Technol., 51, 4289–4296, https://doi.org/10.1021/acs.est.6b05736, 2017.

Squizzato, S., Masiol, M., Brunelli, A., Pistollato, S., Tarabotti, E., Rampazzo, G., and Pavoni, B.: Factors determining the formation of secondary inorganic aerosol: a case study in the Po Valley (Italy), Atmos. Chem. Phys., 13, 1927–1939, https://doi.org/10.5194/acp-13-1927-2013, 2013.

Stavroulas, I., Bougiatioti, A., Grivas, G., Paraskevopoulou, D., Tsagkaraki, M., Zarmpas, P., Liakakou, E., Gerasopoulos, E., and Mihalopoulos, N.: Sources and processes that control the submicron organic aerosol composition in an urban Mediterranean environment (Athens): a high temporal-resolution chemical composition measurement study, Atmos. Chem. Phys., 19, 901–919, https://doi.org/10.5194/acp-19-901-2019, 2019.

Tao, Y. and Murphy, J. G.: The sensitivity of $PM_{2.5}$ acidity to meteorological parameters and chemical composition changes: 10-year records from six Canadian monitoring sites, Atmos. Chem. Phys., 19, 9309–9320, https://doi.org/10.5194/acp-19-9309-2019, 2019.

Theodosi, C., Markaki, Z., and Mihalopoulos, N.: Iron speciation, solubility and temporal variability in wet and dry deposition in the Eastern Mediterranean, Marine Chemistry, 120, 100–107, https://doi.org/10.1016/j.marchem.2008.05.004, 2008.

Tsiflikiotou, M. A., Kostenidou, E., Papanastasiou, D. K., Patoulias, D., Zarmpas, P., Paraskevopoulou, D., Diapouli, E., Kaltsonoudis, C., Florou, K., Bougiatioti, A., Stavroulas, I., Theodosi, C., Kouvarakis, G., Vasilatou, V., Siakavaras, D., Biskos, G., Pilinis, C., Eleftheriadis, K., Gerasopoulos, E., Mihalopoulos, N., and Pandis, S. N.: Summertime particulate matter and its composition in Greece, Atmospheric Environment, 213, 597–607, https://doi.org/10.1016/j.atmosenv.2019.06.013, 2019.

Vierke, L., Ahrens, L., Shoeib, M., Palm, W.-U., Webster, E. M., Ellis, D. A., Ebinghaus, R., and Harner, T.: In situ air–water and particle–water partitioning of perfluorocarboxylic acids, perfluorosulfonic acids and perfluorooctyl sulfonamide at a wastewater treatment plant, Chemosphere, 92, 941–948, https://doi.org/10.1016/j.chemosphere.2013.02.067, 2013.

Warner, J. X., Wei, Z., Strow, L. L., Dickerson, R. R., and Nowak, J. B.: The global tropospheric ammonia distribution as seen in the 13-year AIRS measurement record, Atmos. Chem. Phys., 16, 5467–5479, https://doi.org/10.5194/acp-16-5467-2016, 2016.

Weber, R. J., Guo, H., Russell, A. G., and Nenes, A.: High aerosol acidity despite declining atmospheric sulfate concentrations over the past 15 years, Nature Geosci, 9, 282–285, https://doi.org/10.1038/ngeo2665, 2016.

Wexler, A. S.: Atmospheric aerosol models for systems including the ions H^+, NH_4^+, Na^+, SO_4^{2-}, NO_3^-, Cl^-, Br^-, and H_2O, J. Geophys. Res., 107, 4207, https://doi.org/10.1029/2001JD000451, 2002.

Zaveri, R. A., Easter, R. C., Fast, J. D., and Peters, L. K.: Model for Simulating Aerosol Interactions and Chemistry (MOSAIC), J. Geophys. Res., 113, D13204, https://doi.org/10.1029/2007JD008782, 2008.

Zhang, A., Wang, Y., Zhang, Y., Weber, R. J., Song, Y., Ke, Z., and Zou, Y.: Modeling the global radiative effect of brown carbon: a potentially larger heating source in the tropical free troposphere than black carbon, Atmos. Chem. Phys., 20, 1901–1920, https://doi.org/10.5194/acp-20-1901-2020, 2020.

798
799
800
801
802
803
804
805
806
807
808
809
810
811
812
813
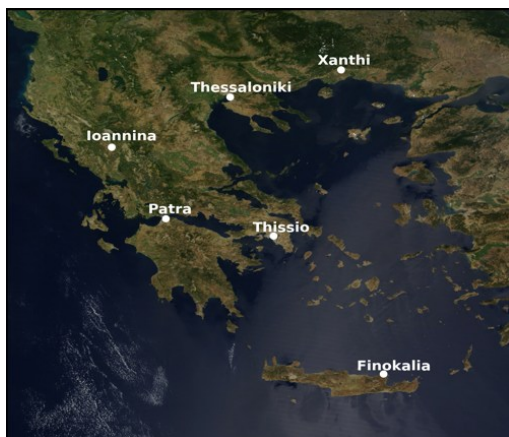
Figure 1: Map of the region of Greece and the sampling sites. From south to north, Finokalia (FKL), Thissio (THI), Patras (PTR), Ioannina (IOA), Thessaloniki (LAP) and Xanthi (XAN). Original satellite image of Greece obtained from (https://upload.wikimedia.org/wikipedia/commons/9/92/Satellite_image_of_Greece.jpg)

814
815
816

817 **Table 1: Descriptive statistics (mean ± stdev) for the chemical composition of $PM_{2.5}$ during the winter and summer**
818 **PANACEA campaigns. *OA* is the *organic aerosol* derived from OC measurements and a ratio of OA/OC of 1.8.**
819 **Meteorological conditions are also provided. (*) The aerosol pH and LWC calculated with ISORROPIA-lite are also**
820 **provided (n= number of days).**

Observations	FKL		THI		PTR	IOA		LAP	XAN
μg/m³	winter	summer	winter	summer	winter	winter	summer	winter	winter
OA	0.69 ± 0.49	2.91 ± 1.10	4.77 ± 4.53	7.51 ± 5.27	17.35 ± 7.61	50.36 ± 34.46	5.06 ± 1.77	12.45 ± 7.97	6.78 ± 3.33
Na⁺	0.39 ± 0.25	0.46 ± 0.33	0.24 ± 0.11	0.17 ± 0.13	0.32 ± 0.30	0.19 ± 0.11	0.12 ± 0.06	0.46 ± 0.49	0.14 ± 0.38
NH₄⁺	0.20 ± 0.25	0.99 ± 0.37	0.40 ± 0.25	1.46 ± 0.50	0.67 ± 0.43	1.12 ± 0.81	0.79 ± 0.33	1.04 ± 0.76	0.75 ± 0.58
K⁺	0.18 ± 0.24	0.25 ± 0.13	0.29 ± 0.24	0.12 ± 0.05	0.75 ± 0.43	1.45 ± 1.00	0.27 ± 0.18	0.37 ± 0.17	0.30 ± 0.16
Ca²⁺	0.27 ± 0.40	0.18 ± 0.14	0.23 ± 0.24	0.23 ± 0.20	0.34 ± 0.44	0.96 ± 0.78	0.55 ± 0.25	0.33 ± 0.11	0.17 ± 0.06
Mg²⁺	0.10 ± 0.12	0.06 ± 0.03	0.02 ± 0.02	0.06 ± 0.01	0.03 ± 0.04	0.03 ± 0.02	0.04 ± 0.01	0.04 ± 0.01	0.04 ± 0.02
SO₄²⁻	1.30 ± 0.59	3.71 ± 1.18	0.77 ± 0.43	4.42 ± 1.59	1.78 ± 0.90	2.77 ± 1.42	3.27 ± 1.02	2.05 ± 1.00	1.90 ± 1.36
NO₃⁻	0.30 ± 0.30	0.14 ± 0.11	0.66 ± 0.50	0.16 ± 0.09	1.39 ± 0.78	3.66 ± 2.73	0.17 ± 0.07	2.01 ± 1.71	0.70 ± 0.58
Cl⁻	0.37 ± 0.47	0.31 ± 0.30	0.40 ± 0.19	0.40 ± 0.12	0.25 ± 0.27	0.61 ± 0.38	0.26 ± 0.07	0.33 ± 0.14	0.40 ± 0.18
T (°C)	11.83 ± 2.74	24.84 ± 1.66	10.64 ± 3.22	28.97 ± 1.90	11.14 ± 2.36	7.43 ± 2.52	26.86 ± 2.60	9.94 ± 2.65	8.62 ± 2.90
RH (%)	72.03 ± 9.68	65.82 ± 9.66	65.85 ± 11.65	46.04 ± 6.69	64.66 ± 11.97	68. 06 ± 20.25	51.59 ± 9.73	57.62 ± 13.17	62.43 ± 16.88
Month (number of samples)	January (n=16)	July & August (n=34)	January (n=27)	July & August (n=34)	January (n=16)	January (n=27)	July & August (n=34)	January (n=4)	January (n=26)
pH*	3.25 ± 0.37	2.08 ± 0.37	3.30 ± 0.48	1.38 ± 0.18	3.70 ± 0.45	4.08 ± 0.42	1.82 ± 0.65	3.01 ± 0.31	2.81 ± 0.53
LWC (μg/m³)*	6.85 ± 3.65	5.85 ± 3.05	3.06 ± 2.96	3.34 ± 1.62	7.00 ± 5.36	56.61 ± 127.59	1.97 ± 0.79	29.68 ± 32.67	4.57 ± 4.29

821
822
823
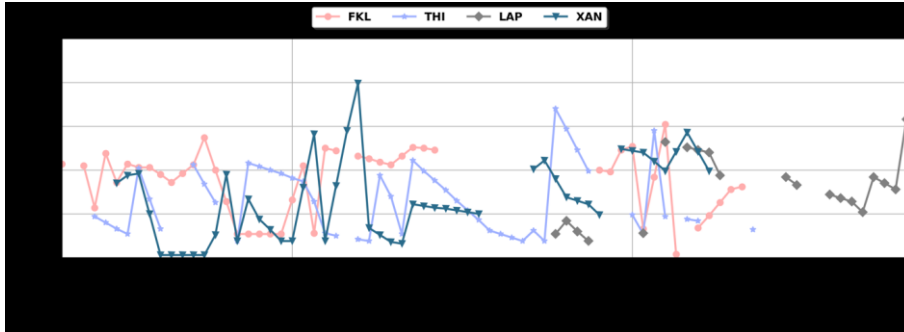
824
825 **Figure 2: Daily surface NH₃ concentrations during the winter of 2019-2020 as derived from the Cross-track Infrared**
826 **Sounder (CrIS) instrument for FKL, THI, LAP and XAN.**

827

828
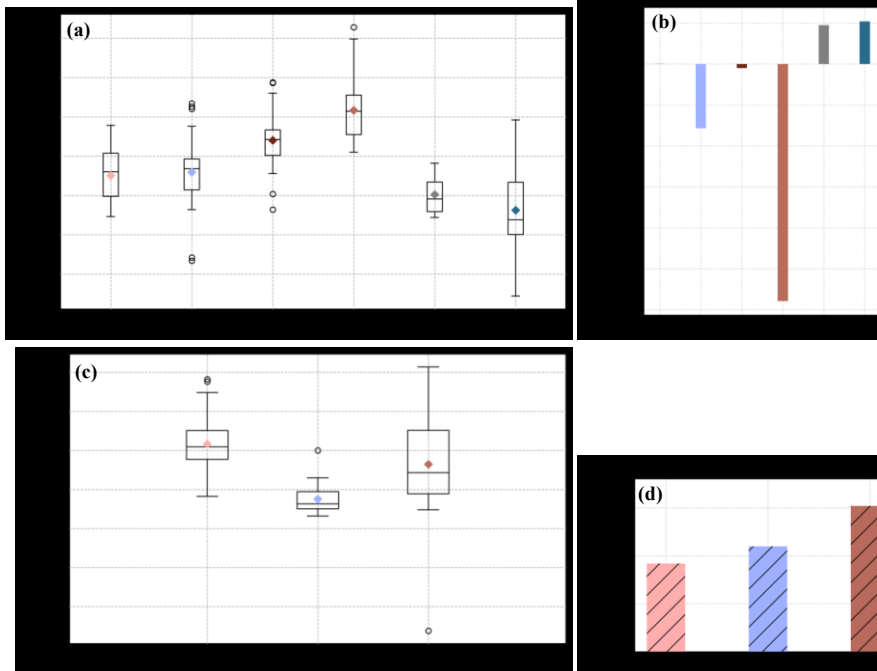
830
831 **Figure 3: a) and c) total aerosol pH (meaning the aerosol pH associated with inorganics and organics) derived using**
832 **ISORROPIA-lite in January 2020 and summer 2019 (July and August) respectively, b) and d) ΔpH = total aerosol pH**
833 **– inorganic aerosol pH both derived from ISORROPIA-lite in January 2020 and summer 2019 respectively. The**
834 **inorganic aerosol pH was derived by setting the organic concentration and hygroscopicity as zero.**
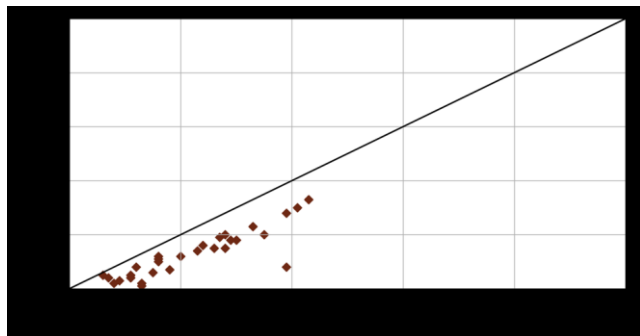
835
836 **Figure 4: Evaluation of the ISORROPIA-lite results for the case of PTR in winter. Comparison of the partitioning**
837 **coefficient of NH$_4$$^+$ calculated from measurements with that from the predicted concentrations derived from the model**
838 **(R^2 = 0.78 and y = 0.70x - 0.03). The partitioning coefficient is defined as ε(NH$_4$$^+$) = NH$_4$$^+$/(NH$_4$$^+$ + NH$_3$).** *The black line*
839 *shows the 1:1 ratio.*

840

841

842

843

844 (a)

845 (b)
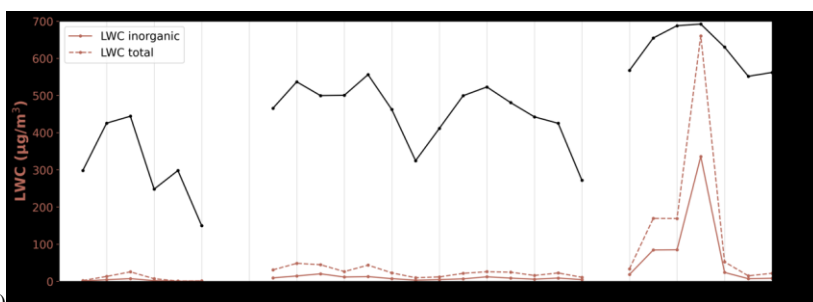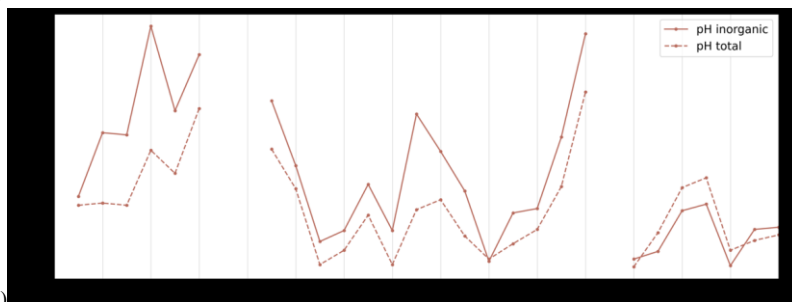
846 **Figure 5: (a) Aerosol liquid water content at IOA in January 2020 as derived from ISORROPIA-lite associated with**
847 **inorganics (inorganic,** *red line***), associated with both inorganics and organics (total,** *red- dashed line***) and relative**
848 **humidity levels (secondary y axis,** *black line***). (b) Inorganic** *(red line)* **and total (***red dashed line,* **associated with**
849 **inorganics and organics) aerosol pH at IOA in January 2020.**

850

851

852

853

854

855

856

857

858

859

860 **Figure 6: Mean fine aerosol pH in winter and in summer at (a) IOA (c) THI, (e) FKL and the respective sensitivity**
861 **results for winter conducted for each site (Tables S5 - S7). $\Delta pH_{abs} = |pH_{winter} - pH_{winter(summerX)}|$, where summerX is the**
862 **mean summer temperature (first simulation, S_1), relative humidity (S_2), TNO_3 (S_3), TNH_3 (S_4), SO_4^{2-} (S_5), Na^+ (S_6), K^+**
863 **(S_7), Ca^{2+} (S_8) and OA concentration (S_9) in IOA (b), THI (d) and FKL (f).**

(a)   (b)
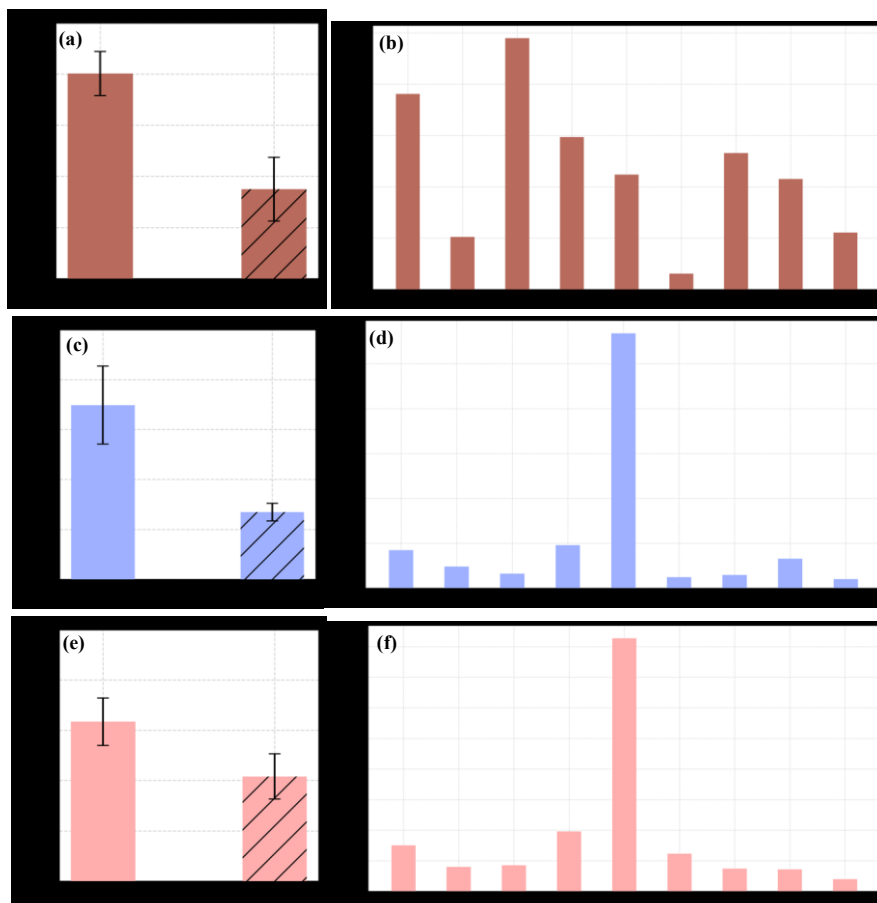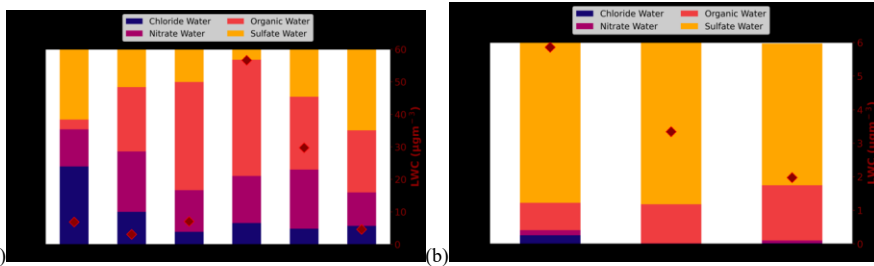
Figure 7: Averaged aerosol liquid water content (LWC) for all sites in winter, January 2020 (a) and summer, July and August 2019 (b) expressed as the contribution of each chemical aerosol salt group considering both the inorganics and organics at the observational sites shown in Fig. 1 (left axis). Aerosol water mean concentrations are shown with rhombus in each plot (right axis).
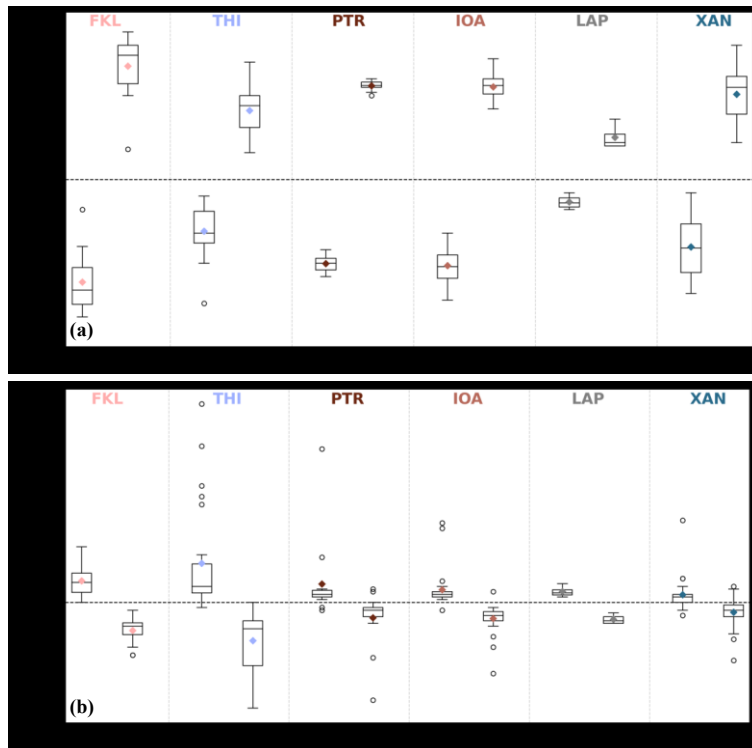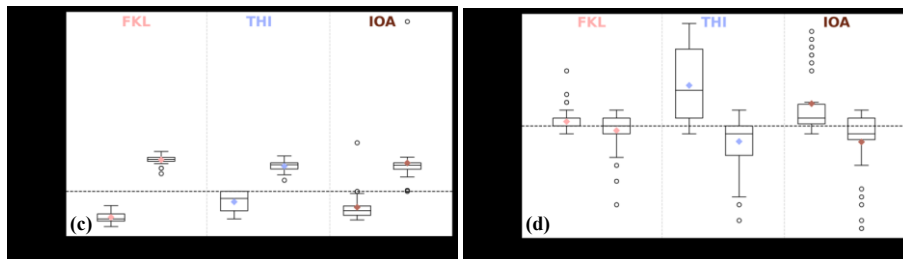
Figure 8: Sensitivity of pH estimation to gas phase NH₃ and HNO₃ concentrations. (a) and (b) are the wintertime (January) simulations for NH₃ and HNO₃ tests respectively and (c) and (d) for the summertime ones (July and August). Each graph shows the difference in pH when using half or double the concentration of the respective gas compared to the original pH at each site. (ΔpH = pH$_{1/2gas}$ − pH$_{original}$ and ΔpH = pH$_{x2gas}$ − pH$_{original}$ respectively).

(a) (b)
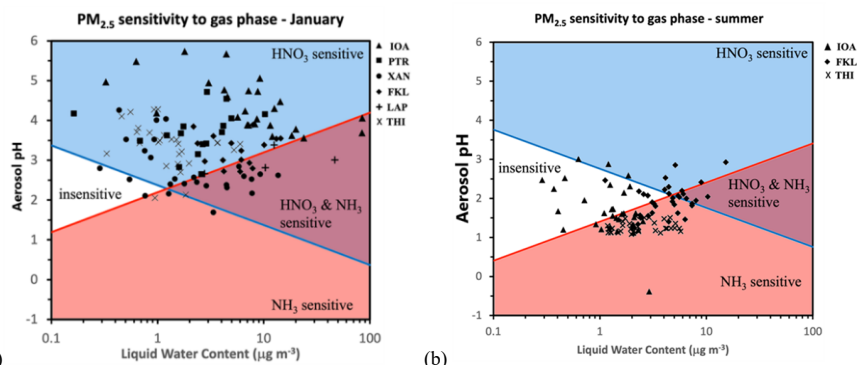
Figure 9: Chemical domains of sensitivity of PM$_{2.5}$ *mass* to NH₃ and NO$_x$ emissions for the studied period (a) in winter (January) and (b) in summer (July and August). The average temperature used here is the mean measured one for the studied period at all sites in each season. Daily averaged values in each season of aerosol pH and liquid water content were used. *The red line shows the characteristic aerosol pH as a function of liquid water content below which the PM$_{2.5}$ mass is sensitive to NH₃ levels and the blue line the characteristic aerosol pH as a function of liquid water content above which the PM$_{2.5}$ mass is sensitive to HNO₃ levels.*

902 (a)   (b)
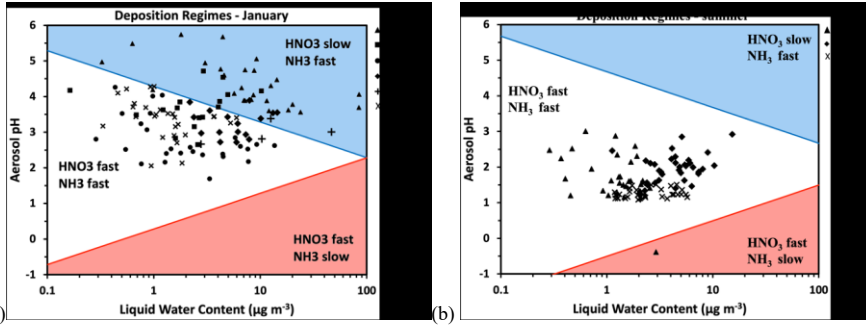
Figure 10: Domains of reactive nitrogen deposition for the studied period (a) in winter (January) and (b) in summer
(July and August). The average temperature used here is the mean measured one at all sites, for each season. Daily
averaged values in each season for aerosol pH and liquid water content were used. *The red line shows the characteristic
aerosol pH, as a function of liquid water content, below which NH₃ deposition is slow and the blue line the characteristic
aerosol pH, as a function of liquid water content, above which HNO₃ deposition is slow.*